Geophysical Prospecting EAGE EUROPEAN ASSOCIATION OF GEOSCIENTISTS & ENGINEERS

Geophysical Prospecting doi: 10.1111/j.1365-2478.2011.00991.x

Iterative electromagnetic migration for 3D inversion of marine controlled-source electromagnetic data

Michael S. Zhdanov[1,2], Martin Čuma[1,2], Glenn A. Wilson[1]*, Evgeny P. Velikhov[3], Noel Black[1] and Alexander V. Gribenko[1,2]

[1]*TechnoImaging, 4001 South, 700 East, Suite 500, Salt Lake City, UT 84107, USA,* [2]*University of Utah, 115 South, 1460 East, Room 383, Salt Lake City, UT 84112, USA, and* [3]*Russian Research Center Kurchatov Institute, 1 Akademika Kurchatova pl., Moscow 123182, Russia*

Received December 2010, revision accepted June 2011

ABSTRACT

The key to deriving a reliable quantitative interpretation from marine controlled-source electromagnetic data is through the integration of shared earth modeling and robust 3D electromagnetic inversion. Subsurface uncertainty is minimized through efficient workflows that use all available subsurface data as a priori information and which permit multiple resistivity models to explain the same observed data. To this end, we present our implementation of an iterative migration method for controlled-source electromagnetic data that is equivalent to rigorous 3D inversion. Our iterative migration method is based on the 3D integral equation method with inhomogeneous background conductivity and focusing regularization with a priori terms. We will show that focusing stabilizers recover more geologically realistic models with sharper resistivity contrasts and boundaries than traditional smooth stabilizers. Additionally, focusing stabilizers have better convergence properties than smooth stabilizers. Finally, inhomogeneous background information described as a priori resistivity models can improve the fidelity of the final models. Our method is implemented in a fully parallelized code. This makes it practical to run large-scale 3D iterative migration on multicomponent, multifrequency and multiline controlled-source electromagnetic surveys for 3D models with millions of cells. We present a suite of interpretations obtained from different iterative migration scenarios for a 3D controlled-source electromagnetic feasibility study computed from a detailed model of stacked anticline structures and reservoir units of the Shtokman gasfield in the Russian sector of the Barents Sea.

Key words: CSEM, Electromagnetics, Inversion, Migration, Regularization, Stabilizer.

INTRODUCTION

The premise of the various marine controlled-source electromagnetic (CSEM) methods is sensitivity to the lateral extents and thicknesses of resistive bodies embedded in conductive hosts. For this reason, CSEM methods were initially applied to de-risking exploration and appraisal with direct hydrocarbon indication. However, CSEM methods represent just one part of an integrated exploration strategy for hydrocarbons. The value of CSEM data is only realized when those models derived from CSEM inversion are integrated, with sound geological understanding, in a shared earth model. The most successful applications of CSEM to date have been in complement to those seismic interpretations where lithological or fluid variations cannot be adequately discriminated by seismic methods alone (Hesthammer *et al.* 2010). Hydrocarbon reserves and resources are estimated with varying confidence

*E-mail: glenn@technoimaging.com

(or risk) from volumetrics calculated from different subsurface models. Confidence is only established through the testing of multiple subsurface models that satisfy all available data. Resistivity models derived from 1D or 2.5D CSEM inversion provide the least confidence because of their inherently reduced dimensionality; those models derived from 3D inversion provide the most confidence.

Here, we distinguish between inversion and interpretation, two terms often used interchangeably. Inversion is a quantitative process whereby a model is recovered from observed data, regardless of whether any a priori knowledge was used or not. Interpretation is a more qualitative process whereby geological insight is inferred from at least one model. CSEM interpretation is inherently reliant upon models derived from inversion methods since CSEM data cannot simply be separated or transformed with linear operators as per seismic methods. Methods for inverting CSEM data are complicated by the very small, non-unique and non-linear responses of hydrocarbon-bearing reservoir units when compared to the total fields.

In 3D CSEM inversion, geological prejudice is introduced via regularization (Tikhonov and Arsenin 1977), whether this is an a priori model, data or model weights, model bounds and/or by the choice of a stabilizing functional (Zhdanov 2002). Most often, resistivity models are obtained from regularization with a smooth stabilizing functional (e.g., Mackie, Watts and Rodi 2007; Commer and Newman 2008; Støren, Zach and Maaø 2008; Ramananjaona and MacGregor 2010). This means the first or second derivatives of the resistivity distribution are minimized, resulting in smooth distributions of the resistivity. These types of solution allegedly satisfy Occam's razor since they are claimed to produce the most 'simplistic' models for the data. Unfortunately, this approach has led to a tendency to deliver a single resistivity model as 'the' solution. Moreover, these classes of models are the least relevant to economic geology, which is anything but smooth. When the resistivity distribution is discontinuous, smooth stabilizers can also produce spurious oscillations and artefacts. Therefore, a model that is smooth in the first or second derivative of the anomalous resistivity distribution is not any 'simpler' than, say, a model that has the minimum volume of the anomalous resistivity distribution. As we will show below, the use of focusing stabilizers allows us to recover stable and geologically realistic models with sharper geoelectric boundaries and contrasts (Fig. 1).

In this paper, we demonstrate that the best practice is to run multiple 3D inversion scenarios with differing regularization in order to enable interpreters to explore alternative 3D resistivity models and to select the most geologically plausible ones for further analysis. Such practice identifies any artefacts that may arise from interpreting a single resistivity model. Alternative models may be used to reveal which additional data, if any, are needed to further constrain the interpretation. To this end, it is important to develop rigorous but fast 3D inversion methods. The requirement for 'fast' 3D inversion makes the various stochastic methods computationally prohibitive. Rigorous inversion methods are also not practical, as the sensitivity matrix needs to be constructed at each iteration for the many transmitter-receiver combinations in a CSEM survey. To minimize computation costs, various incarnations of the Born approximation that linearize the adjoint operators are often used (e.g., Gribenko and Zhdanov 2007; Støren *et al.* 2008). However, for nonlinear inverse problems such approximations can result in inaccurate calculations of the gradient directions, model updates and thus final models. Our more pragmatic approach to 3D CSEM inversion is based on iterative electromagnetic migration. Iterative migration is implemented in a reweighted regularized conjugate gradient method to rigorously compute the gradient directions without needing to explicitly construct the sensitivity matrix or its products (Zhdanov 2002). Modelling is based on the 3D integral equation method with inhomogeneous background conductivity that can capture arbitrary geological complexity. We have implemented our iterative migration method in fully parallelized software that allows us to invert entire 3D CSEM surveys for models with millions of cells. Our approach makes it practical to run multiple inversion scenarios as described above and as we shall demonstrate in our Shtokman case study.

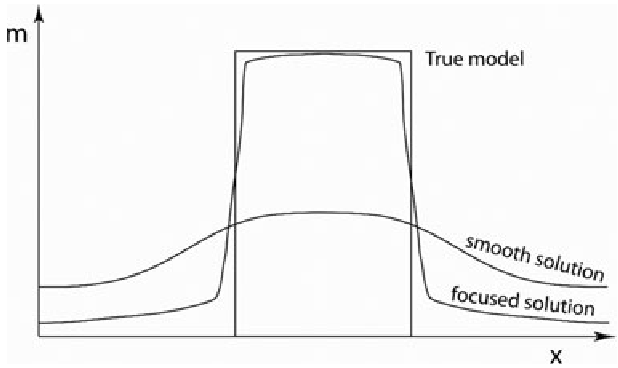

Figure 1 A smooth stabilizer will recover a model with a smooth distribution of model parameters. A focusing stabilizer will recover a model closer to the true model, with sharper boundaries and higher contrasts.

ELECTROMAGNETIC MIGRATION

The physical principles of electromagnetic migration parallel those underlying optical holography and seismic migration; i.e., the recorded fields scattered by an object form a hologram, which one can subsequently use to reconstruct an image of the object by 'illuminating' the hologram with a reference field (Zhdanov 1988). In traditional formulation of migration imaging (e.g., Zhdanov and Čuma 2009), in order to produce the migration field, we replace a set of the receivers with a set of auxiliary transmitters located in the receiver's positions. These transmitters generate an electromagnetic (EM) field, which is called a backscattering or migration field, $\mathbf{E}^m$. The vector cross-power spectrum of the background field, $\mathbf{E}^b$ and the migration field, $\mathbf{E}^m$, produces a numerical reconstruction of a volume image of the conductivity distribution (Zhdanov 2002, 2009). In the case of the marine CSEM method, it is convenient to use a reciprocity principle both for forward modelling and imaging/inversion of the marine CSEM data. In the framework of this approach, the multiple computations of the EM field in the sea-bottom receiver, generated by multiple transmitter positions, is substituted by one calculation of the EM fields in the locations of the true transmitters due to one reciprocal source located in the true receiver position. Taking into account this 'reciprocal' application of the reciprocity method, the principles of marine CSEM migration can be summarized as follows (Zhdanov 2009):

1 We 'illuminate' the background media by a reciprocal electric dipole (in the case of electric observations) located in the positions of the actual receivers to generate the 'electric mode' background EM fields, $\widetilde{\mathbf{E}}^{bE}$ and $\widetilde{\mathbf{H}}^{bE}$. Alternatively, we 'illuminate' the background media by a reciprocal magnetic dipole (in the case of the magnetic field observations) located in the positions of the actual receivers to generate the 'magnetic modes' background EM fields, $\widetilde{\mathbf{E}}^{bH}$ and $\widetilde{\mathbf{H}}^{bH}$.
2 We 'illuminate' the background media by artificial transmitters located in the positions of the true transmitters and represented by equivalent (fictitious) electric current dipoles. In the case of electric observations, the current moments are determined by the complex conjugate anomalous electric field observed in the true receiver for a given transmitter position. The electromagnetic field produced by this system of artificial electric dipoles generates the 'electric mode' migration anomalous fields, $\widetilde{\mathbf{E}}^{mE}$ and $\widetilde{\mathbf{H}}^{mE}$. In the case of magnetic observations, the current moments are determined by the complex conjugate anomalous electric field multiplied by the factor $-i\omega\mu$. The electromagnetic field produced by this system of artificial transmitters generates the 'magnetic mode' migration anomalous fields, $\widetilde{\mathbf{E}}^{mH}$ and $\widetilde{\mathbf{H}}^{mH}$.
3 In the case of electric field observations, the conductivity model of the subsurface $\mathbf{l}_0^E$ is formed by summation of the cross-power spectrum of the 'electric mode' background and migration fields:

$$\mathbf{l}_0^E = \mathrm{Re}\sum_{\omega} \widetilde{\mathbf{E}}^{bE} \cdot \widetilde{\mathbf{E}}^{mE}, \tag{1}$$

where summation is done over all frequencies of the recorded fields.
4 In the case of magnetic field observations, the conductivity model of the subsurface $\mathbf{l}_0^H$ is formed by calculating the cross-power spectrum of the 'magnetic mode' background and migration fields:

$$\mathbf{l}_0^H = \mathrm{Re}\sum_{\omega} \widetilde{\mathbf{E}}^{bH} \cdot \widetilde{\mathbf{E}}^{mH}. \tag{2}$$

5 In the case of joint migration of electric and magnetic observed data, the conductivity model of the subsurface $\mathbf{l}_0^{EH}$ is formed by summation of the 'electric mode' and 'magnetic mode' images

$$\mathbf{l}_0^{EH} = \mathrm{Re}\sum_{\omega} \left[\widetilde{\mathbf{E}}^{bE} \cdot \widetilde{\mathbf{E}}^{mE} + \widetilde{\mathbf{E}}^{bH} \cdot \widetilde{\mathbf{E}}^{mH}\right]. \tag{3}$$

Note that, in the case of multireceiver observations, the final image is produced by summation of all the migration fields generated for each receiver. The conductivity models generated by equations (1)–(3) are usually slightly distorted due to the different spatial sensitivities of the observed data in the model. To account for different sensitivities of the data to the conductivity distribution, we use an additional model weighting function, W_m:

$$\sigma \approx -k(\mathbf{W}_m^* \mathbf{W})^{-1}\mathbf{l}_0, \tag{4}$$

where $\mathbf{l}_0$ stands for any of the migration images introduced above and k is some scaling coefficient. The model parameter weighting matrix $\mathbf{W}_m$ is computed using the integrated sensitivity $\mathbf{S}$ as follows:

$$\mathbf{W}_m = \sqrt{\mathbf{S}}, \tag{5}$$

where the integrated sensitivity is determined from:

$$\mathbf{S} = diag\sqrt{\mathbf{F}^* \mathbf{F}}. \tag{6}$$

In this last equation, $\mathbf{F}$ is the Fréchet matrix of the forward modeling operator. By weighting the migration image $\mathbf{l}_0^{EH}$ with the integrated sensitivity, we make sure that the observed data are equally sensitive to the conductivity variations within every part of the domain of investigation.

Electromagnetic migration for controlled-source electromagnetic methods

Let us consider a typical CSEM survey consisting of a set of electric and magnetic field receivers located on the seafloor and an electric bipole transmitter towed at some elevation above the seafloor. We assume that the electrical conductivity in the model can be represented as the sum of the background conductivity σ_b and an anomalous conductivity $\Delta\sigma$ distributed within some local inhomogeneous domain D associated with the reservoir structures.

The background conductivity is formed by a horizontally layered model that consists of nonconductive air and a layered subsurface including the conductive sea column. The receivers are located at the points $\mathbf{r}_j$, where $j = 1, 2, 3, \ldots, J$, in a Cartesian coordinate system. Every receiver R_j records electric and magnetic field components generated by an electric bipole transmitter moving above the receivers. We denote these observed fields as $\mathbf{E}_i(r_j)$ and $\mathbf{H}_i(r_j)$ where i is the index of the corresponding transmitter T_i located at the point $\mathbf{r}_i$ where $i = 1, 2, 3, \ldots, I$.

Let us consider the data observed by one receiver, R_j. We also introduce two auxilary electric current dipoles, $\mathbf{q}$ and $\mathbf{p}$. According to reciprocity, the electric field component excited at $\mathbf{r}_j$ in the direction of $\mathbf{p}$ by an electric current element $\mathbf{q}$ at $\mathbf{r}_i$ is identical to the electric field component excited at $\mathbf{r}_i$ in the direction of $\mathbf{q}$ by an electric current element $\mathbf{p}$ at $\mathbf{r}_j$ (Zhdanov 2002, p. 226):

$$\mathbf{E}_i(\mathbf{r}_j) \cdot \mathbf{p} = \mathbf{E}_j^E(\mathbf{r}_i) \cdot \mathbf{q}. \tag{7}$$

Similarly, the magnetic field component excited at $\mathbf{r}_j$ in the direction of $\mathbf{p}$ by an electric current element $\mathbf{q}$ at $\mathbf{r}_i$ is equal to the electric field component (multiplied by the minus sign) excited at $\mathbf{r}_i$ in the direction of $\mathbf{q}$ by a magnetic current element $\mathbf{p}$ at $\mathbf{r}_j$:

$$\mathbf{H}_i(\mathbf{r}_j) \cdot \mathbf{p} = -\mathbf{E}_j^H(\mathbf{r}_i) \cdot \mathbf{q}. \tag{8}$$

Therefore, one can substitute a reciprocal survey configuration for the original survey, assuming that we have electric T_j^E and magnetic T_j^H dipole transmitters located in the positions of the receivers, R_j and a set of receivers measuring the reciprocal electric fields $\mathbf{E}_j^E(\mathbf{r}_i)$ and $\mathbf{E}_j^H(\mathbf{r}_i)$ in the positions of the original transmitters, T_i.

We can calculate the migration field for the data collected by one fixed seafloor receiver, R_j. Consider, for example, the reciprocal electric fields $\mathbf{E}_j^E(\mathbf{r}_i)$. These fields can be represented as the sum of the background (b) and anomalous (a) parts:

$$\mathbf{E}_j^E(\mathbf{r}_i) = \mathbf{E}_j^b(\mathbf{r}_i) + \mathbf{E}_j^a(\mathbf{r}_i), \tag{9}$$

where the background electric field $\mathbf{E}_j^b(\mathbf{r}_i)$ is generated by the electric dipole transmitter T_j^E in a model with a background conductivity $\sigma_b(z)$. The residual fields $\mathbf{R}_{E_j}(\mathbf{r}_i)$ are equal to the difference between the background and 'observed' reciprocal field:

$$\mathbf{R}_{E_j}(\mathbf{r}_i) = \mathbf{E}_j^b(\mathbf{r}_i) - \mathbf{E}_j^E(\mathbf{r}_i) = -\mathbf{E}_j^{E_a}(\mathbf{r}_i). \tag{10}$$

According to the definition by Zhdanov (2002, 2009), the migrated residual field is a field generated in the background medium by a combination of all electric dipole transmitters located at points $\mathbf{r}_i$ with current moments determined by the complex conjugate residual field $\mathbf{R}_{E_j}^*(\mathbf{r}_i)$ according to the following:

$$\mathbf{E}_j^m(\mathbf{r}) = \mathbf{E}_j^m(\mathbf{r}; \mathbf{R}_{E_j}^*) = \sum_{i=1}^{I} \widehat{\mathbf{G}}_E(\mathbf{r}, \mathbf{r}_i) \cdot \mathbf{R}_{E_j}^*(\mathbf{r}_i), \tag{11}$$

where the lower subscript j shows that we migrate the field observed by the receiver R_j and $\widehat{\mathbf{G}}_E(\mathbf{r}, \mathbf{r}_i)$ is the electric Green's tensor for the background conductivity model, σ_b. Therefore, the migration field can be computed as a superposition of 1D responses weighted by the corresponding receiver residual and generated by electric dipoles with unit moments located at every transmitter position in the model with background conductivity σ_b. This 1D electric dipole modelling is a very fast process, which results in a fast migration algorithm.

Equation (11) allows us to reconstruct the migration field everywhere in the medium under investigation. It can be shown that this transformation is stable with respect to the noise in the observed data (Zhdanov 2009). At the same time, the spatial distribution of the migration field is closely related to the conductivity distribution in the medium. However, one needs to apply imaging conditions to enhance the conductivity model produced by migration. We will discuss this problem in a later section.

In the general case of multiple receivers, the migration field is generated in the background medium by all electric dipole transmitters located above all receivers, R_j, having current moments determined by the complex conjugate residual field, $\mathbf{R}_{E_j}^*(\mathbf{r}_i)$:

$$\mathbf{E}^m(\mathbf{r}) = \sum_{j=1}^{J} \sum_{i=1}^{I} \widehat{\mathbf{G}}_E(\mathbf{r}, \mathbf{r}_i) \cdot \mathbf{R}_{E_j}^*(\mathbf{r}_i). \tag{12}$$

According to equation (11), we have:

$$\mathbf{E}^m(\mathbf{r}) = \sum_{j=1}^{J} \mathbf{E}_j^m(\mathbf{r}). \tag{13}$$

Therefore, the total migration field for all receivers can be obtained by summation of the corresponding migration field computed for every individual receiver. A remarkable fact is that the migration of both electric and magnetic field data is actually reduced to the same forward problem for the electric field generated by the electric dipole transmitters. The only difference is that, in the case of the electric field receivers, we use the electric observed data to determine the electric current moment in the reciprocal transmitters. In the case of the magnetic receivers, the observed magnetic data are used to determine the electric current moments of the receivers.

Regularized iterative migration

It can be demonstrated that migration can be treated as the first iteration in the solution of an electromagnetic inverse problem (Zhdanov 2009). Obviously, we can obtain better images if we repeat migration iteratively. Following Zhdanov, Čuma and Ueda (2010), we can describe the method of iterative migration as follows: on every iteration, we calculate the predicted electromagnetic response $\widetilde{\mathbf{E}}_n$ for the given conductivity model σ_n, obtained from the previous iteration. We then calculate the residual field between this response and the observed data, $\widetilde{\mathbf{R}}_E^n$, and then we migrate the residual field. The updated conductivity model is obtained, according to equation (1), as a sum over the frequencies of the dot product of the migrated residual field and the predicted electromagnetic response $\widetilde{\mathbf{E}}^n$. This conductivity model is then corrected by the integrated sensitivity **S** to produce the new conductivity model σ_n on the basis of equation (4). The iterative migration is terminated when the residual field becomes smaller than the required accuracy level of the data fitting. In fact, the iterative migration results in rigorous inversion.

It has been demonstrated that migration provides an alternative method for evaluation of adjoint operators. When applied iteratively, migration is analogous to inversion by providing a rigorous solution to the corresponding inverse problem (Zhdanov 2002, 2009).

Note that every iteration of the migration algorithm requires two forward modeling computations: one to compute the migration field and another to compute the predicted data in the receivers. In this work, we use a recently developed migration code that is parallelized over the z dimension of the migration domain. For calculation of the migration and predicted fields, we use the integral equation method with inhomogeneous background conductivity. This enables us to considerably reduce computation time and also model larger problems by increasing the migration domain size and the number of the cells used for the migration domain discretization.

CHOOSING A STABILIZING FUNCTIONAL

Another advantage of iterative migration is based on the fact that it allows us to include an a priori model of the target in the iterative process in a way similar to the case of conventional inversion. The details of this technique can be found in Zhdanov (2002).

Regardless of the iterative scheme used, all our regularized inversions seek to minimize the Tikhonov parametric functional, $P^\alpha(m)$:

$$P^\alpha(m) = \phi(m) + \alpha s(m) \rightarrow \min, \tag{14}$$

where $\phi(m)$ is a misfit functional of the observed and predicted data, $s(m)$ is a stabilizing functional and α is the regularization parameter that balances (or biases) the misfit and stabilizing functional (Zhdanov 2002). The stabilizing functional incorporates information about the class of models used in the inversion. The choice of stabilizing functional should be based on the user's geological knowledge and prejudice. Using an inappropriate type of stabilizer is akin to looking for an inappropriate solution. In this section, we will briefly describe different smooth and focusing stabilizers in order to demonstrate the results from the iterative migration of the same CSEM data produced by each.

A minimum norm (MN) stabilizer will seek to minimize the norm of the difference between the current model and an a priori model:

$$s_{MN}(m) = \int_V (m - m_{apr})^2 dv, \tag{15}$$

and usually produces a relatively smooth model for a difference $(m - m_{apr})$. The Occam (OC) stabilizer implicitly introduces smoothness with the first derivatives of the model parameters:

$$s_{OC}(m) = \int_V (\nabla m - \nabla m_{apr})^2 dv, \tag{16}$$

and produces smooth resistivity models that bear little resemblance to economic geology. Moreover, it can result in spurious oscillations and artefacts when the resistivity is discontinuous.

Alternatively, the use of focusing stabilizers makes it possible to recover models with sharper geoelectric boundaries and contrasts. We briefly describe this recently introduced family of stabilizers here and refer the reader to Zhdanov (2002,

2009) and Zhdanov, Gribenko and Čuma (2008) for further details.

First, we present the minimum support (MS) stabilizer:

$$s_{MS}(m) = \int_V \frac{(m - m_{apr})^2}{(m - m_{apr})^2 + e^2} dv, \tag{17}$$

where e is a focusing parameter introduced to avoid singularity when $m = m_{apr}$. The minimum support stabilizer minimizes the volume with nonzero departures from the a priori model. Thus, a smooth distribution of all model parameters with a small deviation from the a priori model is penalized. A focused distribution of the model parameters is penalized less. Similarly, we present the minimum vertical support (MVS) stabilizer:

$$s_{MVS}(m) = \int_V \frac{(m - m_{apr})^2}{\int_S (m - m_{apr})^2 ds + e^2} dv, \tag{18}$$

where S is a horizontal section from the inversion domain (Zhdanov *et al.* 2008). This minimizes the thickness of the volume with non-zero departures from the a priori model. The MVS stabilizer is specifically designed to invert thin subhorizontal structures, such as hydrocarbon-bearing reservoirs.

Finally, we present the minimum gradient support (MGS) stabilizer:

$$s_{MGS}(m) = \int_V \frac{\nabla(m - m_{apr}) \cdot \nabla(m - m_{apr})}{\nabla(m - m_{apr}) \cdot \nabla(m - m_{apr}) + e^2} dv, \tag{19}$$

which minimizes the volume of model parameters with non-zero gradient.

Note that, the focusing parameter e controls the degree of focusing the inverse images. The smaller the focusing parameter e, the sharper the contrasts of conductivities in the inverse images. However, parameter e should not be too small, because it could result in singularities of the expressions for focusing stabilizers when $m = m_{apr}$. At the same time it should not be too large, because in this case the image will not be focused. Thus, the problem of selecting the focusing parameter e is very similar to the problem of choosing the regularization parameter alpha. Zhdanov and Tolstaya (2004) introduced a method to estimate the optimum value of e, similar to the L-curve method for selection of the regularization parameter α (Hansen 1998).

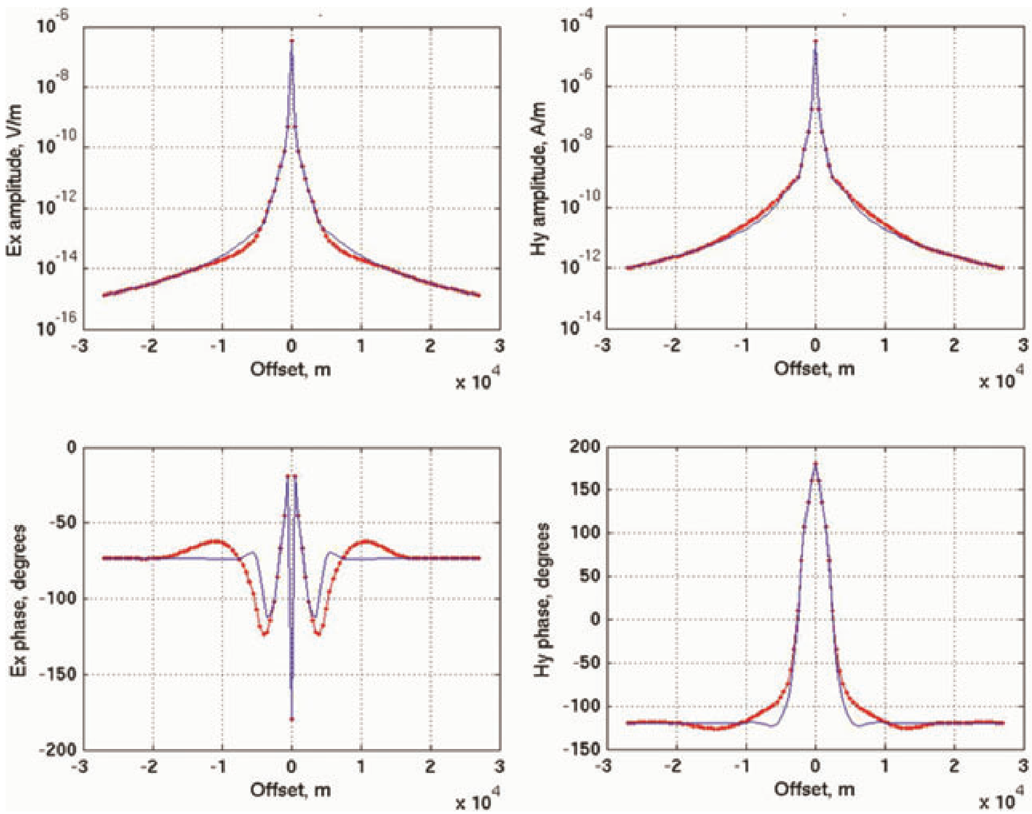

Figure 2 Observed (red) and background (blue) fields for the in-line electric and transverse magnetic field components at a receiver close to the centre of the Shtokman model.

CASE STUDY – SHTOKMAN

The Shtokman gasfield lies in the centre of the Russian sector of the Barents Sea, approximately 500 km north of the Kola Peninsula. It is currently operated by a joint venture between Gazprom, Total and StatoilHydro. Shtokman is one of the world's largest known natural gasfields, with reserves of 3.8 tcm of gas and 37 mln t of gas condensate (Gazprom 2009). The water depth gently varies between 320–340 m over the field. The overburden sequence contains Jurassic and Cretaceous siliciclastics of shallow marine origin. From approximately 1800 m depth, the Shtokman reservoir sequence

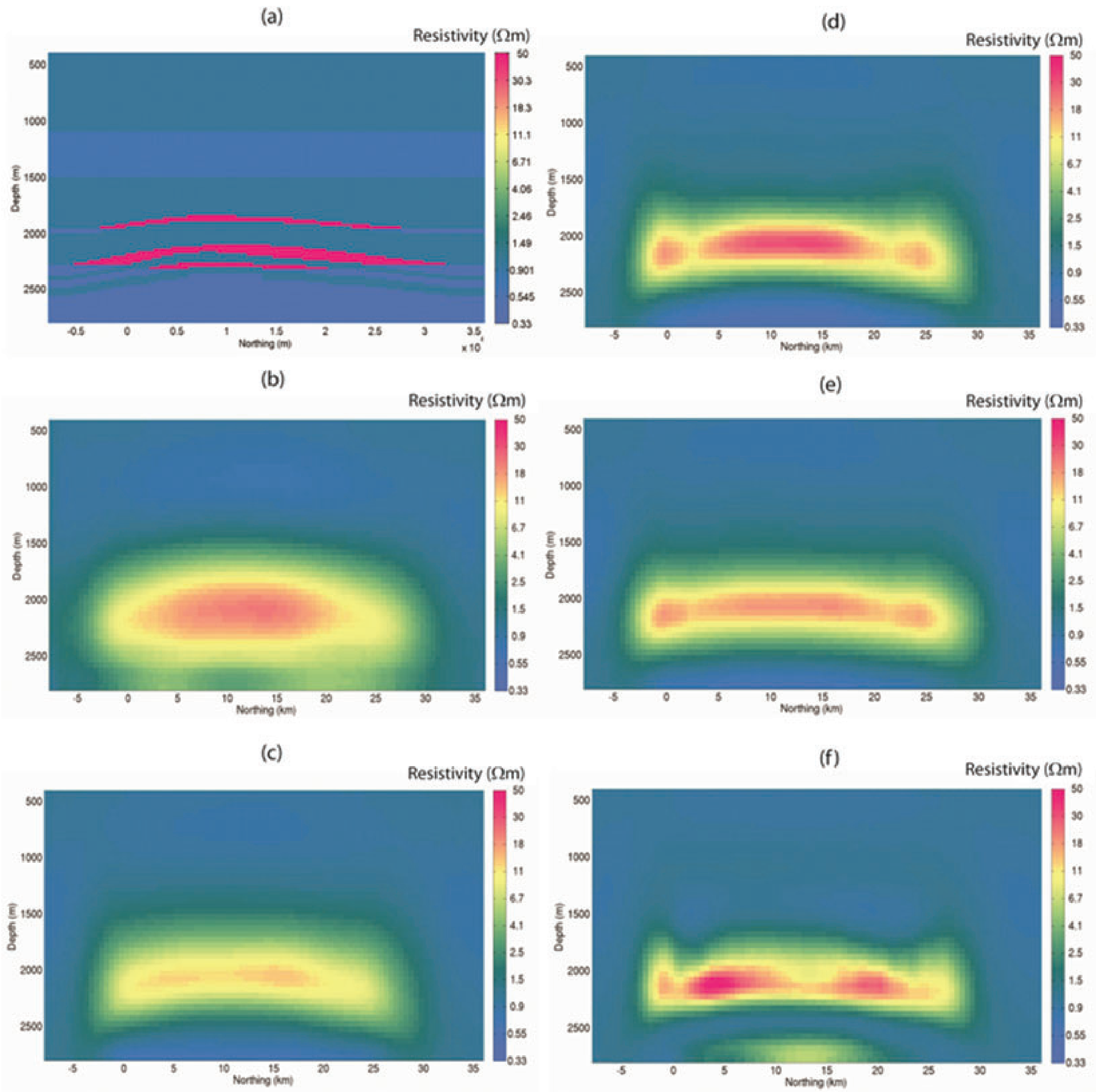

Figure 3 Vertical cross-section of the Shtokman resistivity model obtained from the iterative migration of in-line electric field data with a homogeneous half-space for a) the true resistivity, b) Occam inversion, c) minimum norm, d) minimum support, e) minimum vertical support and f) minimum gradient support. All models fit the observed data within 5.5%.

consists of four Middle and Upper Jurassic sandstone horizons. The gas is trapped in an anticlinal four-way dip structure that is faulted in the crest. The reservoir horizons vary from 10–80 m in thickness. The porosity is between 15–20%, and permeability ranges from hundreds of millidarcies to over a darcy (Zakharov and Yunov 1994).

We constructed a 3D geoelectric model of the Shtokman field from available geological and geophysical information. This model was used to simulate a multifrequency 3D CSEM survey at 0.25 Hz, 0.5 Hz and 0.75 Hz using the 3D integral equation method. The survey consisted of 345 receiver positions distributed over a 2 km × 2 km grid draped over the seafloor. The transmitter was towed 50 m above the seafloor along 50 km long lines that were spaced 2 km apart. For the entire survey, we prepared different combinations of the multifrequency data for migration: in-line electric field only, in-line electric and transverse magnetic fields and in-line and vertical electric and transverse magnetic fields. No noise was added to any of the data, so we could effectively compare the performance of each stabilizer.

As noted in the introduction, the anomalous fields are generally very weak compared to the background fields in the CSEM measurements. Figure 2 shows the observed and background fields for a receiver near the centre of the Shtokman field. The observed field, which includes the anomaly contribution, shows only a small departure from the background signature at offsets under 10 km for the E_x and H_y components. For the E_z component the difference is larger but the magnitude of the amplitude is much smaller.

A number of iterative migration scenarios were considered. In each, the model domain was 44 km × 40 km × 3 km in easting and northing and at depth. The migration was done on a grid with a cell size of 200 m by 200 m in the horizontal directions and with a relatively fine vertical size of 20 m. Thus, the vertical cell size of the migration grid was smaller than the 50–100 m thicknesses of the reservoir layers. The data sets corresponding to each data combination were then migrated with different stabilizers: Occam (OC), minimum norm (MN), minimum support (MS), minimum vertical support (MVS), and minimum gradient support (MGS). The focusing parameter was equal to 1e-12 for all the stabilizers. For the purpose of benchmarking performance, all scenarios were run to a common misfit of 5.5%. In the first part of our study, all scenarios commenced with no a priori models so as to not bias the effectiveness of any stabilizer. With no a priori model, we do not expect to be able to resolve the stacked reservoir units of the Shtokman gasfield. What we do expect, however, is to recover a feature with a general shape and a conductivity-thickness product that is comparable to the stacked reservoir units. This is a well-known limitation of the CSEM method's resolution.

Figures 3, 5 and 6 present the results for the different iterative migration scenarios at their final iterations. Though the actual resistivity models are 3D, we show only common vertical cross-sections through each model for ease of visual inspection of model quality. Panel (b) of Fig. 3 shows that iterative migration of the E_x component only with the Occam stabilizer converged to produce a very smooth resistivity model,

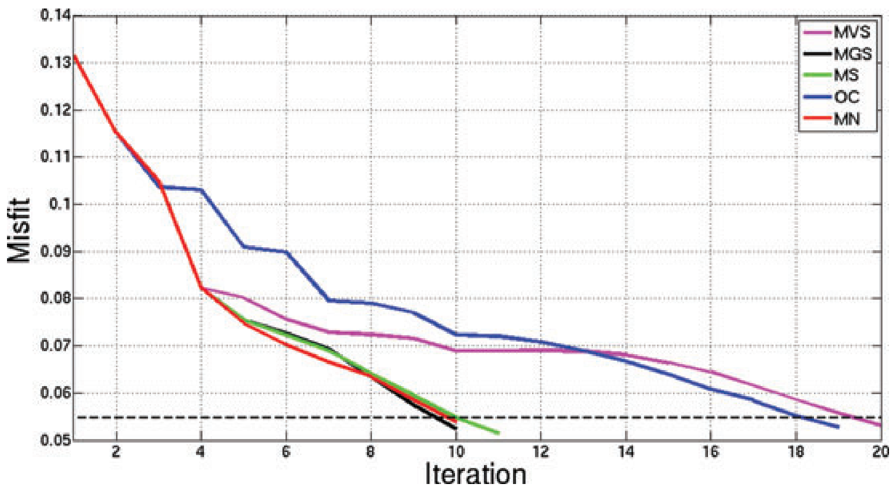

Figure 4 Convergence of misfit for inversion of in-line electric field data with minimum vertical support (MVS), minimum gradient support (MGS), minimum support (MS), Occam (OC) and minimum norm (MN) stabilizers.

one that bears the least resemblance to the actual resistivity model as shown in panel (a) of the same figure. As shown in panel (c) of the same figure, iterative migration with the minimum norm stabilizer also produced a smooth resistivity model. Models with sharper geoelectric boundaries and contrasts were obtained using the family of focusing stabilizers, as shown in panels (d)–(f). Migration with the minimum support, minimum vertical support and minimum gradient support stabilizers produced compact resistivity models. These resistivity models bear the most geological relevance to the actual geology, as they recovered the anticlinal trends of the Shtokman reservoir units. As expected, the minimum vertical support

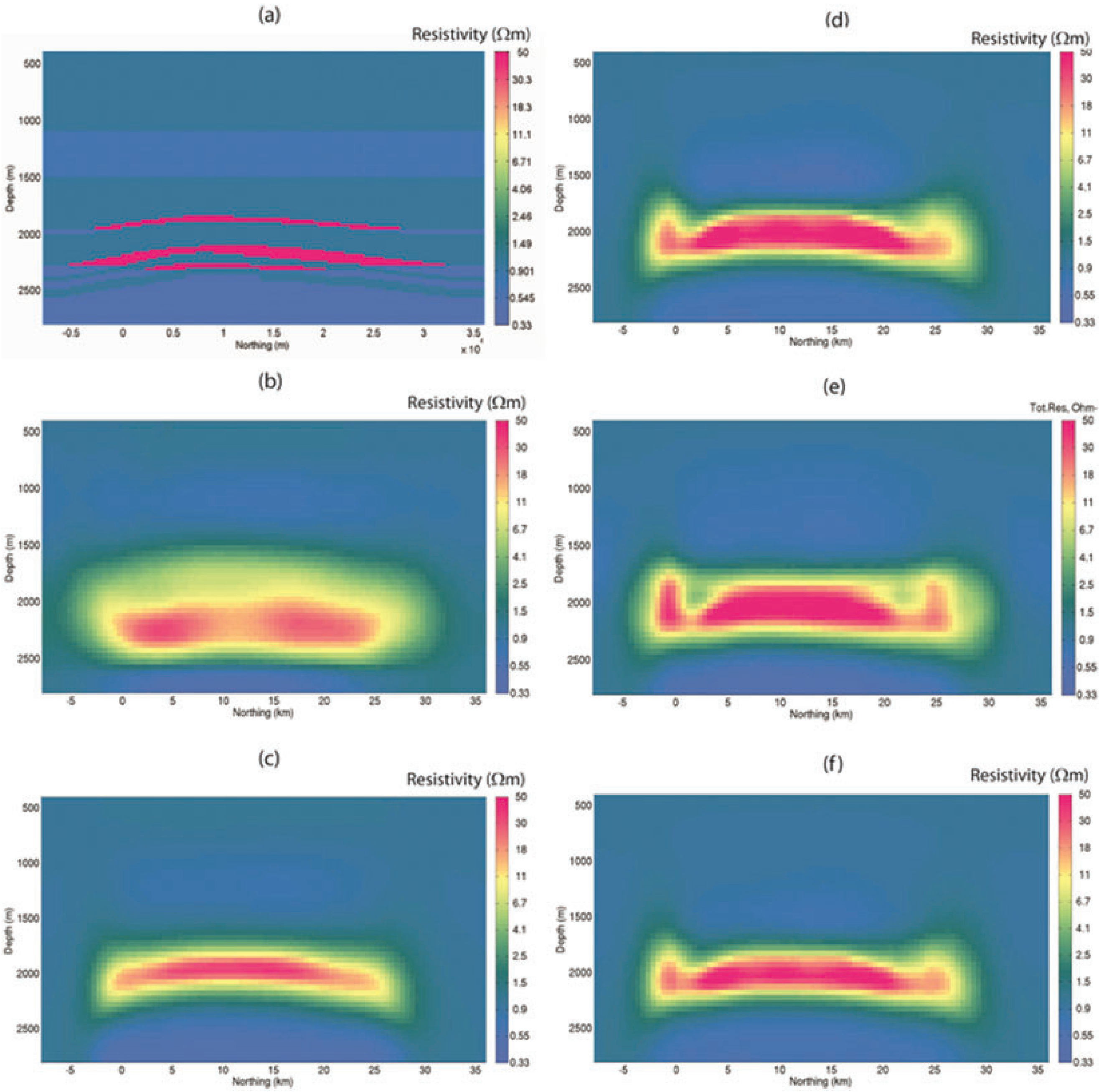

Figure 5 Vertical cross-section of the Shtokman resistivity model obtained from the iterative migration of in-line electric field and transverse magnetic field data with a homogeneous half-space for a) the true resistivity, b) Occam inversion, c) minimum norm, d) minimum support, e) minimum vertical support and f) minimum gradient support. All models fit the observed data within 5.5%.

recovered the thinnest resistivity model. The minimum gradient support spreads the anomaly out somewhat in an effort to account for the multiple stacked true anomalies. As shown in Figs 5 and 6, addition of the H_y and E_z components improves the Occam and minimum norm results but they still produce overly smooth models.

We have compared the convergence of the inversion misfit, which we define as the norm of difference between the normalized observed and predicted data (Fig. 4). This result is representative of the other scenarios whereby all stabilizers exhibited near-quadratic convergence. As shown in previous figures, our results show that there is noticeable improvement

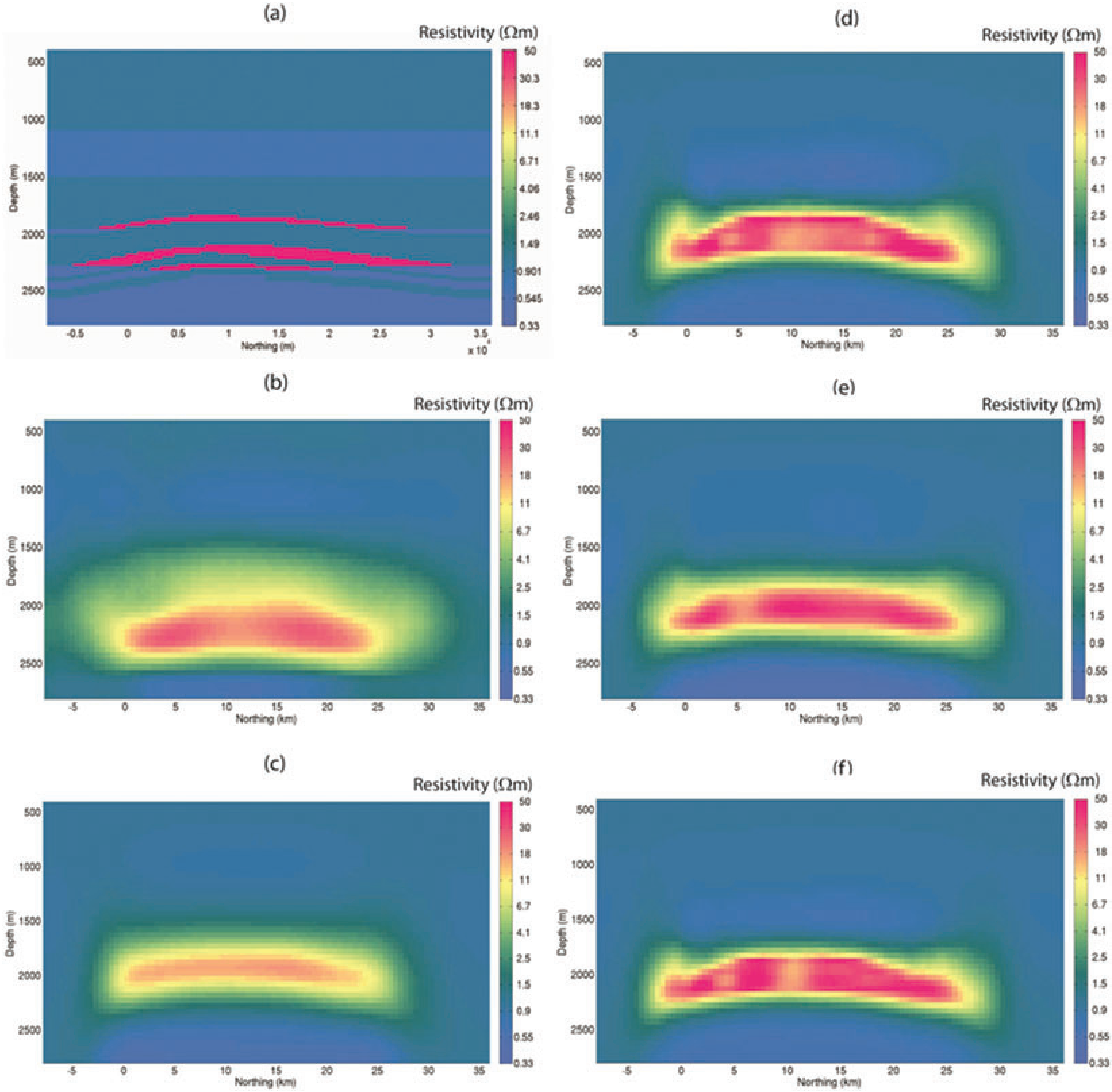

Figure 6 Vertical cross-section of the Shtokman resistivity model obtained from the iterative migration of in-line and vertical electric field and transverse magnetic field data with a homogeneous half-space for a) the true resistivity, b) Occam inversion, c) minimum norm, d) minimum support, e) minimum vertical support and f) minimum gradient support. All models fit the observed data within 5.5%.

in the quality of the recovered resistivity models as the transverse magnetic and then vertical electric fields are added to the CSEM data prepared for migration. It follows that, as the industry moves towards acquiring 3D surveys with the intent of defining 3D structure, the ability to invert all components of data along multiple lines for 3D resistivity models will prove to be essential.

In the second part of our study, we evaluate the use of an inhomogeneous background resistivity model rather than a homogeneous half-space (Zhdanov and Čuma 2009). We

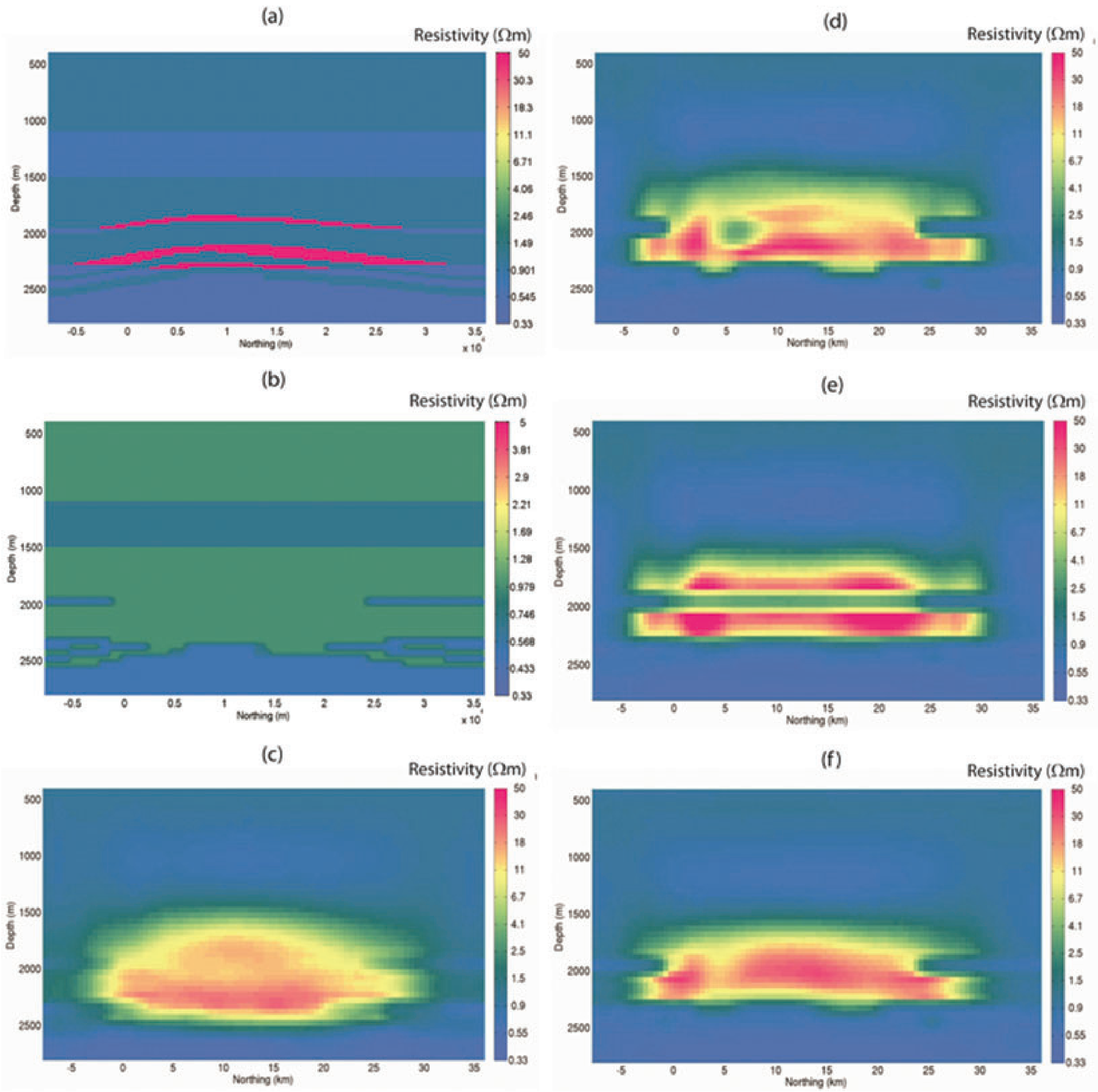

Figure 7 Vertical cross-section of the Shtokman resistivity model obtained from the iterative migration of in-line and vertical electric field and transverse magnetic field data with an inhomogenous a priori model for a) the true resistivity, b) inhomogeneous a priori resistivity, c) Occam inversion, d) minimum support, e) minimum vertical support and f) minimum gradient support. All models fit the observed data within 5.5%.

constructed an inhomogeneous background resistivity model from the original resistivity model but removed the reservoirs so as to present the anticlinal structures. Again, we ran iterative migration for all types of stabilizers and data combinations. Figure 7 shows results for iterative migration of the E_x, H_y, and E_z data. Interestingly, the stacked reservoir units emerge from the smooth stabilizers but are far better defined with the focusing stabilizers. In Fig. 8, we compare models obtained using the minimum vertical support stabilizer for different data combinations. It is remarkable that it is possible to recover stacked resisters in these images that correlate to the stacked reservoir horizons.

CONCLUSION

3D inversion of CSEM data is inherently nonunique; multiple models will satisfy the same observed data. Multiple inversion scenarios must be investigated in order to explore different a priori models, data combinations and stabilizers, all with the intention of minimizing subsurface uncertainty. For such practicality, it is important to use rigorous but fast 3D inversion methods. Our approach to this is based on iterative migration, theoretically equivalent to but more efficient than iterative inversion. As we have demonstrated with our synthetic example for the Shtokman field, we are able to effectively invert multicomponent, multifrequency and multiline CSEM surveys for models with millions of cells. This makes it practical to run multiple scenarios in order to build confidence in the robustness of features in the resistivity models, as well as to discriminate any artefacts that may arise from the interpretation of a single resistivity model. We have shown that reliance on regularization with smooth stabilizers may produce resistivity models that bear little resemblance to petroleum geology. We have shown that focusing stabilizers recover more

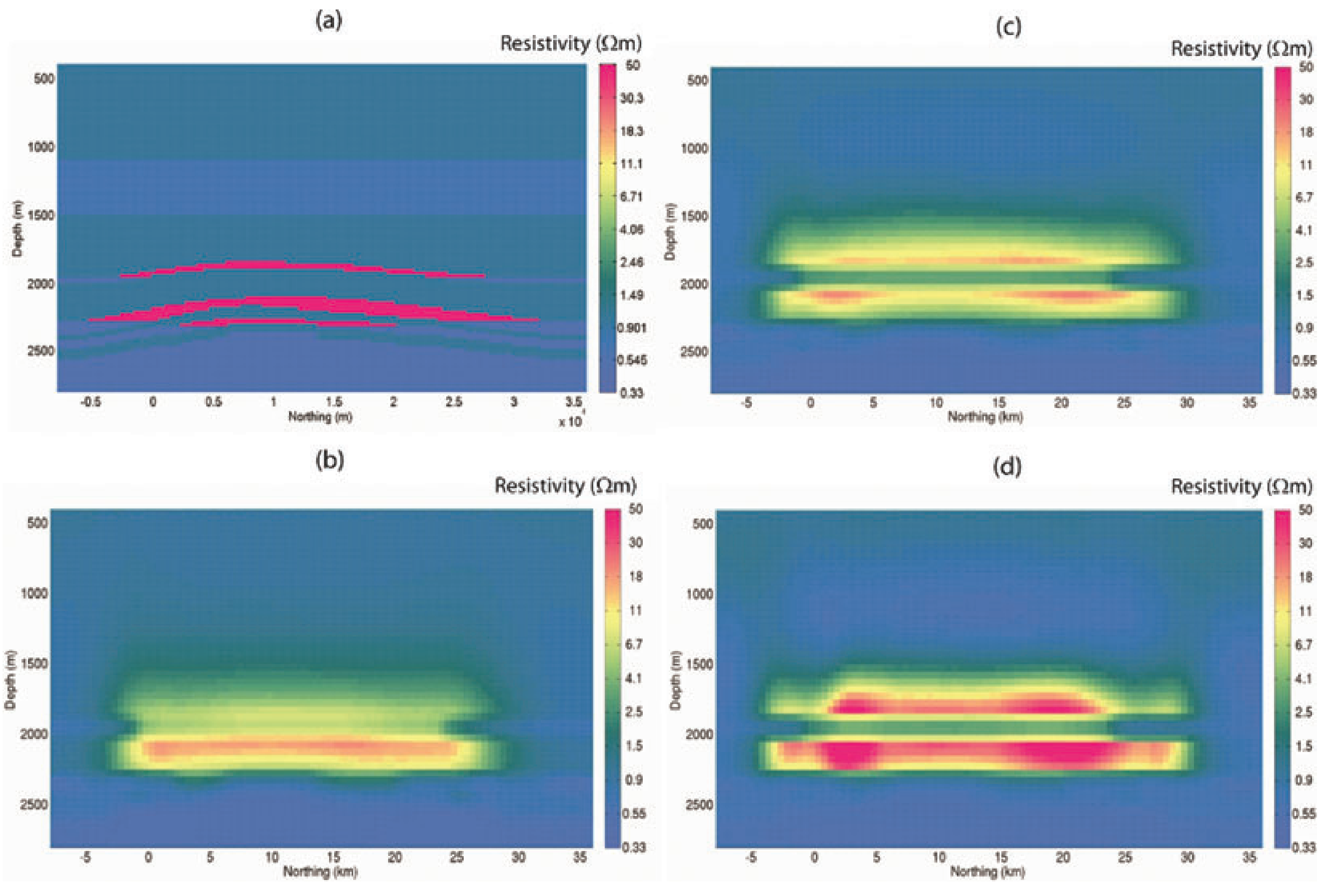

Figure 8 Vertical cross-section of the Shtokman resistivity model obtained from the iterative migration using the minimum vertical support stabilizer with an inhomogeneous a priori model for a) the true resistivity, b) inversion of in-line electric field data, c) inversion of in-line electric field and transverse magnetic field data and d) inversion of in-line and vertical electric field and transverse magnetic field data. All models fit the observed data within 5.5%.

realistic resistivity models with sharper geoelectric contrasts and converge to lower misfits in fewer iterations. Finally, using a known non-horizontally layered structure as an inhomogeneous background resistivity a priori model to the iterative migration can improve model fidelity and recover stacked reservoir units. In order to extract the most reliable information from geophysical data, multiple inversion scenarios should be applied and the inversions should be run both with different a priori models and with different regularization parameters. The final selection of the most geologically meaningful model should be based on integrated analysis/interpretation of all available geological and/or geophysical information in the area of investigation.

ACKNOWLEDGEMENTS

The authors acknowledge TechnoImaging for support of this research and permission to publish. The authors acknowledge the Russian Research Centre Kurchatov Institute for assistance in preparation of the Shtokman geoelectric model. M. Zhdanov, M. Čuma and A. Gribenko also acknowledge the support of the University of Utah's Consortium for Electromagnetic Modeling and Inversion (CEMI) and Center for High Performance Computing (CHPC).

REFERENCES

Commer M. and Newman G.A. 2008. New advances in controlled source electromagnetic inversion. *Geophysical Journal International* **172**, 513–535. doi: 10.1111/j.1365-246X.2007.03663.x

Gazprom. 2009. http://old.gazprom.ru/eng/articles/article21712.shtml (accessed 19 December 2009).

Gribenko A. and Zhdanov M.S. 2007. Rigorous 3D inversion of marine CSEM data based on the integral equation method. *Geophysics* **72**, WA73–WA84. doi: 10.1190/1.2435712

Hansen C. 1998. *Rank-deficient and Discrete Ill-posed Problems: Numerical Aspects of Linear Inversion*. SIAM Monographs on Mathematical Modeling and Computation, SIAM.

Hesthammer J., Stefatos A., Boulaenko M., Fanavoll S. and Danielsen J. 2010. CSEM performance in light of well results. *The Leading Edge* **29**, 34–41. doi: 10.1190/1.3284051

Mackie R., Watts M.D. and Rodi W. 2007. Joint 3D inversion of CSEM and MT data. 77th SEG meeting, San Antonio, Texas, USA, Expanded Abstracts, 574. doi:10.1190/1.2792486

Ramananjaona C. and MacGregor L.M. 2010. 2.5D anisotropic inversion of marine CSEM survey data – an example from West Africa. 72nd EAGE meeting, Rome, Italy, Expanded Abstracts.

Støren T., Zach J.J. and Maaø F.A. 2008. Gradient calculations for 3D inversion of CSEM data using a fast finite-difference time-domain modeling code. 72nd EAGE meeting, Rome, Italy, Expanded Abstracts.

Tikhonov A.N. and Arsenin Y.V. 1977. *Solution of Ill-posed Problems*. Winston.

Zakharov Y.V. and Yunov A.Y. 1994. Direction of exploration for hydrocarbons in Jurassic sediments on the Russian shelf of the Barents Sea. *Geologiya Nefti i Gaza* **2**, 13–15.

Zhdanov M.S. 1988. *Integral Transforms in Geophysics*. Springer Verlag.

Zhdanov M.S. 2002. *Geophysical Inverse Theory and Regularization Problems*. Elsevier.

Zhdanov M.S. 2009. *Geophysical Electromagnetic Theory and Methods*. Elsevier.

Zhdanov M.S. and Čuma M. 2009. Electromagnetic migration of marine CSEM data in areas with rough bathymetry. 79th SEG meeting, Houston, Texas, USA, Expanded Abstracts, 684. doi:10.1190/1.3255847

Zhdanov M.S., Gribenko A. and Čuma M. 2008. Regularized focusing inversion of marine CSEM data using minimum vertical support stabilizer. 78th SEG meeting, Las Vegas, Nevada, USA, Expanded Abstracts, 597. doi:10.1190/1.2792487

Zhdanov M.S., Čuma M. and Ueda T. 2010. 3D electromagnetic holographic imaging in active monitoring of sea-bottom geoelectric structures. In: *Active Geophysical Monitoring* (eds J. Kasahara, V. Korneev and M.S. Zhdanov), pp. 317–342. Elsevier.

Zhdanov M.S. and Tolstaya E. 2004. Minimum support nonlinear parameterization in the solution of 3D magnetotelluric inverse problem. *Inverse Problems* **20**, 937–952.